Welding in the World
https://doi.org/10.1007/s40194-022-01334-0

RESEARCH PAPER

Modification of Co–Cr alloys to optimize additively welded microstructures and subsequent surface finishing

Antonia Eissel[1] · Lorenz Engelking[2] · Kai Treutler[1] · Volker Wesling[1] · Dirk Schröpfer[2] · Thomas Kannengießer[2]

Received: 15 October 2021 / Accepted: 15 June 2022

Abstract
Cobalt chromium alloys are often used in turbine and plant construction. This is based on their high thermal and mechanical stress resistance as well as their high wear resistance to corrosive and abrasive loads. However, cobalt is a cost-intensive material that is difficult to machine. Moreover, increasingly complex structures and the optimisation of resource efficiency also require additive manufacturing steps for the production or repair of components in many sectors. Concerning inhomogeneity and anisotropy of the microstructure and properties as well as manufacturing-related stresses, a lot of knowledge is still necessary for the economic use of additive welding processes in SMEs. As a result of the high stresses on the components and requirements for a high surface quality, a complementary use of additive and machining manufacturing processes is necessary. Thereby, Co–Cr alloys are extremely challenging for machining with geometrically defined cutting edges because of their low thermal conductivity combined with high strength and toughness. An approach to solve this problem is to refine and homogenise the microstructure. This is achieved by modifying the alloy with elements zirconium and hafnium, which are added up to a maximum of 1 wt.-%. A reduction of the process forces and stresses on the tool and work piece surface is also achievable via hybrid milling processes. There are already studies on the combined use of additive and machining manufacturing processes based on laser technology. However, knowledge based on powder and wire-based arc processes is important, as these processes are more widespread. Furthermore, the effects on the surface zone of additively manufactured components by hybrid finish milling have not yet been a subject of research. The results show that the structural morphology could be significantly influenced with the addition of zirconium and hafnium.

Keywords Modification of structural morphology · Co–Cr-alloy · Plasma-transferred arc welding · Ultrasonic-assisted milling

1 Introduction

Due to increasing requirements relating to the efficiency of highly stressed components in turbine or plant construction, the use of cost-intensive, difficult-to-process materials is increasingly necessary today. In this context, cobalt-chromium alloys in particular are highly resistant to thermal and mechanical stress, as well as to corrosive and abrasive loads [1, 2]. CoCr25Ni9Mo stands out in this case because of its excellent wear resistance even at high temperatures of 800 °C [2]. Pure cobalt has allotropic properties depending on the temperature. At high temperatures, it has a face-centred cubic (FCC) crystal structure and at low temperatures a hexagonal close-packed (HCP) crystal structure [3–5]. Therefore, elements are added to stabilise the respective structure. For FCC, Ni, Fe, Mn and C are added, while for HCP structure, W, Cr, Si and Mo are effective [6]. Furthermore, the oxidation and corrosion resistance are ensured by the content of 25 wt.% chromium. In combination with this, chromium is the main carbide creator and generates carbides in the form of M_7C_3, but also $M_{23}C_6$ [7, 8]. This results in an increase in strength [9]. Tungsten and molybdenum are

Recommended for publication by Commission C-IX - Behaviour of Metals Subjected to Welding

✉ Antonia Eissel
antonia.eissel@tu-clausthal.de

Lorenz Engelking
lorenz.engelking@bam.de

[1] Institute of Welding and Machining (ISAF), Agricolastraße 2, 38678 Clausthal-Zellerfeld, Germany

[2] Federal Insitute for Material Research and Testing (BAM), Unter den Eichen 87, 12205 Berlin, Germany

Published online: 05 July 2022

used for solid solution strengthening. In both cases, these additives affect the solidification behaviour, influencing the morphology of the carbides and, moreover, eutectic carbide is formed [1, 10]. M_6C-carbides and MC carbides are formed at the molybdenum and/or tungsten contents [7, 11]. However, the metal cobalt is still one of the most expensive raw materials mainly due to its limited occurrence in the middle of the African continent and increasing use in battery applications. Therefore, the effort to optimise resource efficiency as well as to realise complex structures is increasing. The focus in many areas is moving towards additive manufacturing for the production or repair of components [12]. Additively welded components exhibit inhomogeneous and anisotropic microstructures and properties. As a result, a lot of knowledge is still necessary regarding these characteristics as well as the manufacturing-related stresses for the economic use of additive welding processes in SMEs [12]. In order to produce defined complex structures and functional surfaces that meet the requirements, additively manufactured components usually have to be subsequently surface finished. In the case of metals, this will be usually done by machining with geometrically defined cutting edges, i.e. turning and milling [13]. Co–Cr alloys are considered hard to cut due to low thermal conductivity combined with high material strength and toughness, leading to high challenges for machining steps [14]. In addition, the heterogeneous microstructure and anisotropic properties of additively manufactured components lead to unstable cutting conditions and inconstant cutting forces during machining [15]. Recent studies on the refinement of the morphology structure based on investigations with melting furnaces show that microalloying additions with elements such as zirconium and hafnium produce a homogeneous microstructure, as exemplified by FeNi36 [16]. Zr and Hf are monocarbide-forming reactive elements that generate separate block-shaped particles, such as diamonds or cubes [1], which influence the microstructure. In this paper, the effects of refining elements by means of an arc-based welding process on the cobalt-base alloy CoCr26Ni9Mo5W are investigated. The aim is to achieve a uniform and homogeneous microstructure with a welding process that ensures stable conditions for subsequent cutting processes.

Lizzul et al. have investigated the influence of the build-up direction of Ti-6Al-4 V components manufactured via laser powder bed fusion (L-PBF) on the tool wear during slot milling and showed that the tool wear differs by up to 40% depending on the direction of cutting to the direction of build-up. Lowest tool wear was observed when machining perpendicular to the build-up direction [17]. In addition, also for Ti-6Al-4 V and L-PBF, Lizzul et al. investigated the effect of AM-induced microstructure on the surface integrity by varying the scanning strategy and subsequent turning of the AM-components. They found that the scanning strategy has a significant influence on the microstructure, which in reverse influences the surface integrity due to machining [18]. Note that a sufficient surface integrity is a central requirement for highly stressed safety-relevant components. Influences on surface integrity are a subject of complex interactions between topographical, e.g. surface defects; mechanical, e.g. residual stresses, and metallurgical, e.g. microstructural alterations, effects [19]. Significant improvements in surface integrity, especially for hard-to-cut materials like Co–Cr alloys, can be achieved by using hybrid machining processes, such as ultrasonic-assisted milling (USAM). In USAM, the movement of the cutting edge is superimposed with an additional ultrasonic oscillation and amplitudes in the range of a few micrometres. Rinck et al. observed an increase in surface quality and a significant reduction in cutting forces for USAM compared to a conventional milling process when machining Ti-6Al-4 V. The authors explain the decreasing cutting forces with a discontinuous cutting edge engagement due to superimposed tool tip movement in cutting direction, additionally, leading to a reduction of friction between tool and workpiece [20]. Similar observations for the same material were made by Ni et al. [21]. Liu et al. also observed a significant reduction in cutting forces during USAM of in situ TiB_2/7050Al metal matrix composites compared to the conventional milling process. The authors mainly attribute the cutting force reduction to the supplementary acceleration of the chip due to the ultrasonic oscillation [22].

In this present work, the influence of adding small amounts of hafnium and zirconium to the microstructure of the CoCr26Ni9Mo5W alloy (hereinafter Co–Cr initial alloy) is investigated. Furthermore, the machinability depending on the alloy modification is studied and compared with a hybrid machining process in addition to the conventional process.

2 Material and methods

2.1 Materials used

In order to realise a homogeneous and isotropic microstructure, alloy modifications were made to the Co–Cr initial alloy. The chemical composition of the initial alloy is shown in Table 1, provided by means of powder by company Deloro Wear Solutions GmbH.

For this purpose, hafnium and zirconium were added at different weight percentages according to a statistical experimental design in order to determine the positive effect of the elements on the microstructure morphology as a function of their concentration. The design of experiments is shown in Fig. 1.

The degree of purity and grain size of the welding additives are listed in Table 2. In order to realise the different

Table 1 Alloying elements CoCr26Ni9Mo5W in wt.-%

Alloy	*Co*	*Cr*	*Ni*	*Mo*	*W*	*Fe*	*Mn*	*Si*
CoCr26Ni9Mo5W	54	26	9	5	2	3	0.8	0.3

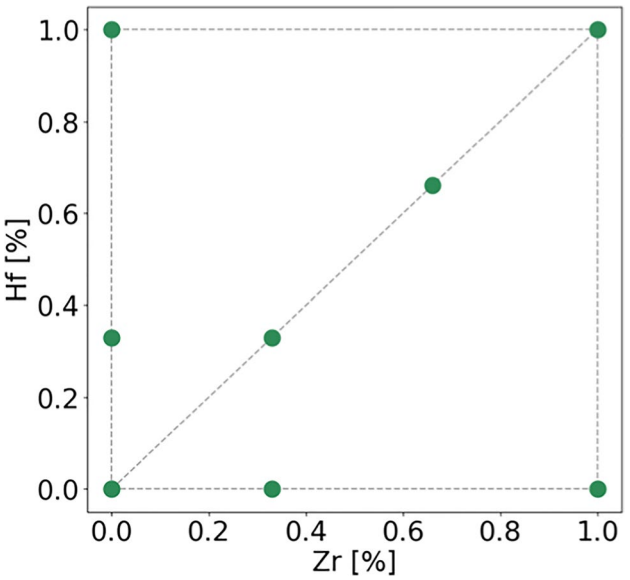

Fig. 1 Design of experiments for alloy modifications

Table 2 Properties of the additives

Alloy	*Purity*	*Particle size*
Zirconium	99.8%	75–150 µm
Hafnium	99.9%	< 100 µm

powder modifications, the 3D shaker mixer TURBULA® was used, leading to a homogeneous mixture due to rotational and translational movements and inversion.

2.1.1 Experimental setup

Plasma-transferred-arc was used for the welding tests. A welding system from Hettiger Schweißtechnik GmbH was applied for this purpose. A sandblasted plate of low-alloy steel S355 was chosen as the substrate plate. The plate was clamped onto a direct cooling plate in order to realise the required low interlayer temperatures. For the investigation of the alloy modifications, wall structures with the dimensions (50 (length) × 50 (width) × 18 (height)) mm^3 were welded in order to perform microstructure and hardness measurements, and the machining investigations can be performed. On the substrate, several single-layer overlapping weld beads were unidirectional welded on top of each other performing a pendulum movement to achieve the specified width. The interlayer temperature was 100 °C. All specimens were welded using argon + 6.5% H_2 with a welding current of approx. 120 A. All welding parameters are listed in Table 3.

Table 3 Welding parameters

Shielding gas	Ar 4.6 + 6.5% H_2
Welding current	120 A
Arc height control	30 V
Welding speed	15 cm/min
Width of pendulum	18 mm
Intermediate layer temperature	100 °C

2.1.2 Metallurgical analysis and hardness measurements

A cross-section disc was then cut from the wall structure for the specimen preparation via wire EDM. The cross-section was divided into three parts and thus categorised into upper, middle and lower layers. The samples were embedded, ground and polished for the light microscopic images. For a sufficiently high contrast ratio of the microstructure images, the samples were etched for approx. 20 s with Beraha II [23]. The images themselves were taken with the light microscope CRT 6 LED from Leica. Using the IMS Client software from Imagic Bildverarbeitung AG, the porosity of the microstructure can be measured and classified. To determine the chemical composition, an EDX (Energy Dispersive X-ray Spectroscopy) analysis was done on a Cambridge Series 4 CamScan.

In addition, the hardness measurement of the welded samples was performed on the DuroScan G5 series hardness testing machine. For this purpose, a series of hardness measurements were conducted over the entire sample cross-section with HV 0.2. Subsequently, five measurements with HV 10 were taken at different points of the cross-section, shown as an example in Fig. 2.

2.2 Machining experiments

In order to investigate the influence of the modification of the Co–Cr initial alloy on subsequent finishing milling conditions, machining experiments without lubrication were carried out on the initial alloy and on the modified alloys with 1% Hf and 1% Zr on a 5-axis machining centre (DMU 65 by DMG MORI) modified for ultrasonic-assisted milling. The tool oscillates at high frequency of 38.1 kHz in the axial direction of the tool at an amplitude of < 10 µm. The experimental setup is

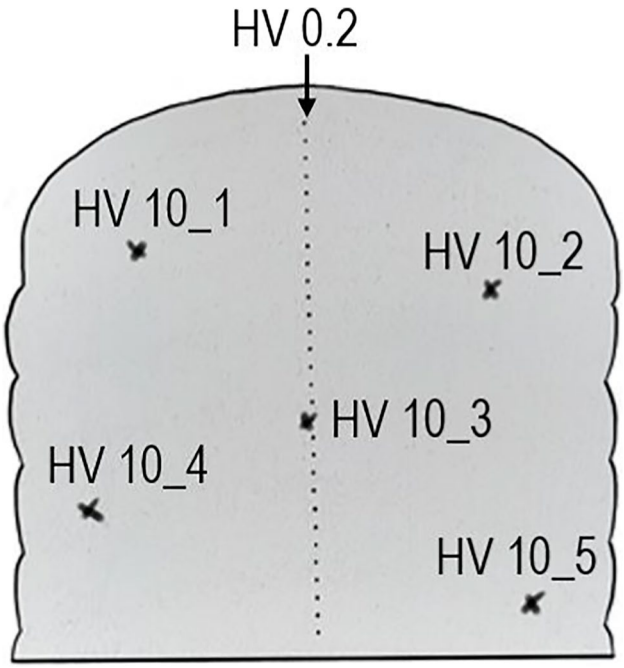

Fig. 2 Hardness measurement using the example of the upper layers

shown in Fig. 3a. The extraction of machining specimens from the AM walls was accomplished by electrical discharge machining (EDM) in as-welded condition with dimensions of approx. 16 mm × 16 mm × 2 mm (length × width × height), cf. Figure 3b. The milling tool for the experiments was a PVD-coated (TiAlN/TiSiN-based) solid carbide ball end mill with a diameter of 6 mm and four flutes (by WOLF Werkzeugtechnik GmbH). Table 4 shows the applied milling parameters. The tests were carried out in down milling with and without ultrasonic-assistance for each alloy modification, and both processes were performed with one milling tool,

Table 4 Experimental data

Cutting speed $v_c = 30$ m/min	*Feed rate* $f_z = 0.04$ mm/tooth	*Ultrasonic assistance* $P_{US} = 0\%$ and 100%
Angle in x-direction $\lambda = 45°$	*Step over* $a_p = 0.3$ mm	*Ultrasonic frequency* $F_{US} = 38.1$ kHz
Angle in y-direction $\tau = 45°$	*Cutting engagement* $a_e = 0.3$ mm	*Amplitude* $\hat{u} = 0.15\ \mu m \pm 0.2\ \mu m$

resulting in six milling parameter and material combinations and two milling tools for the tests.

2.2.1 Cutting force analysis

The cutting forces occurring in the *x*- (feed force F_f), *y*- (feed normal force F_{fN}) and *z*-directions (passive force F_p) were measured during the finish milling experiments using a dynamometer (9139AA by KISTLER, time resolution: 0.1 ms). A resulting cutting force F_r was calculated according to formula 1:

$$F_r = \sqrt{F_f^2 + F_{fN}^2 + F_p^2} \tag{1}$$

2.2.2 Surface analysis

In order to investigate the influence of the modification of the Co–Cr initial alloy and the two machining processes of conventional milling and USAM on the surface integrity, the arithmetic mean roughness *Ra* was first determined in accordance with the standard DIN EN ISO 4287 normal to the feed direction using a contact profilometer (HOMMEL-ETAMIC T1000 by JENOPTIK) [24]. In addition, images for the surface analysis were taken using a light microscope (VHX-7000 by KEYENCE).

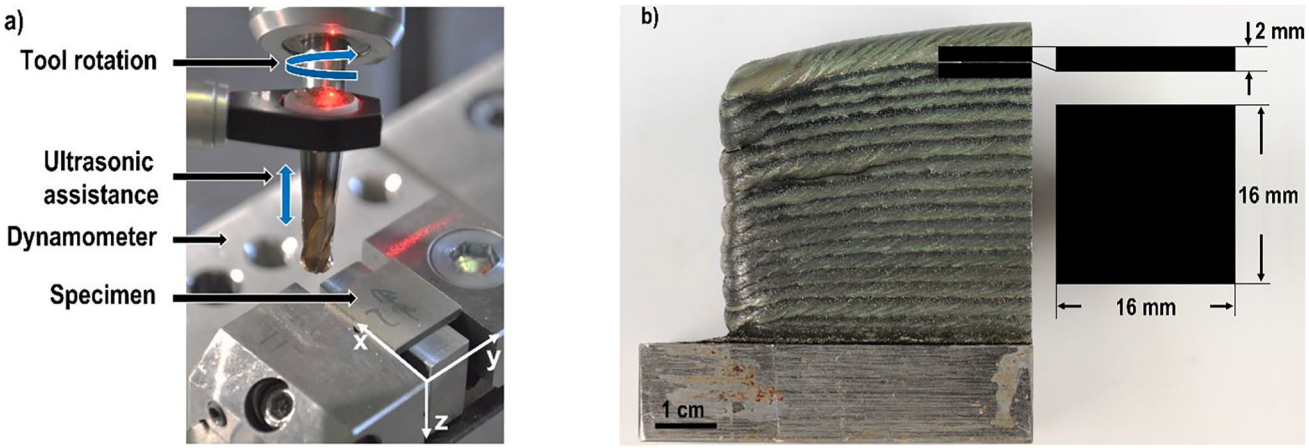

Fig. 3 **a** Experimental setup, **b** the exemplary sampling and the specimen dimensions

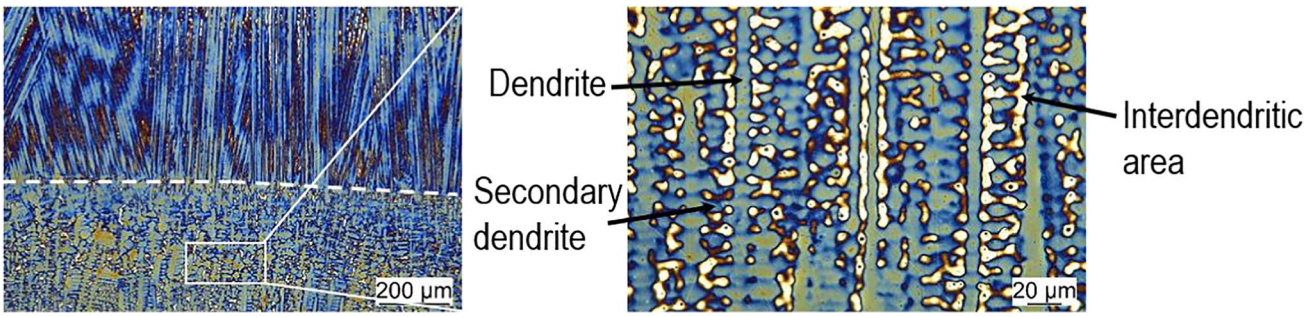

Fig. 4 Microstructure of CoCr26Ni9Mo5W with different magnifications: left 100x, right 500x

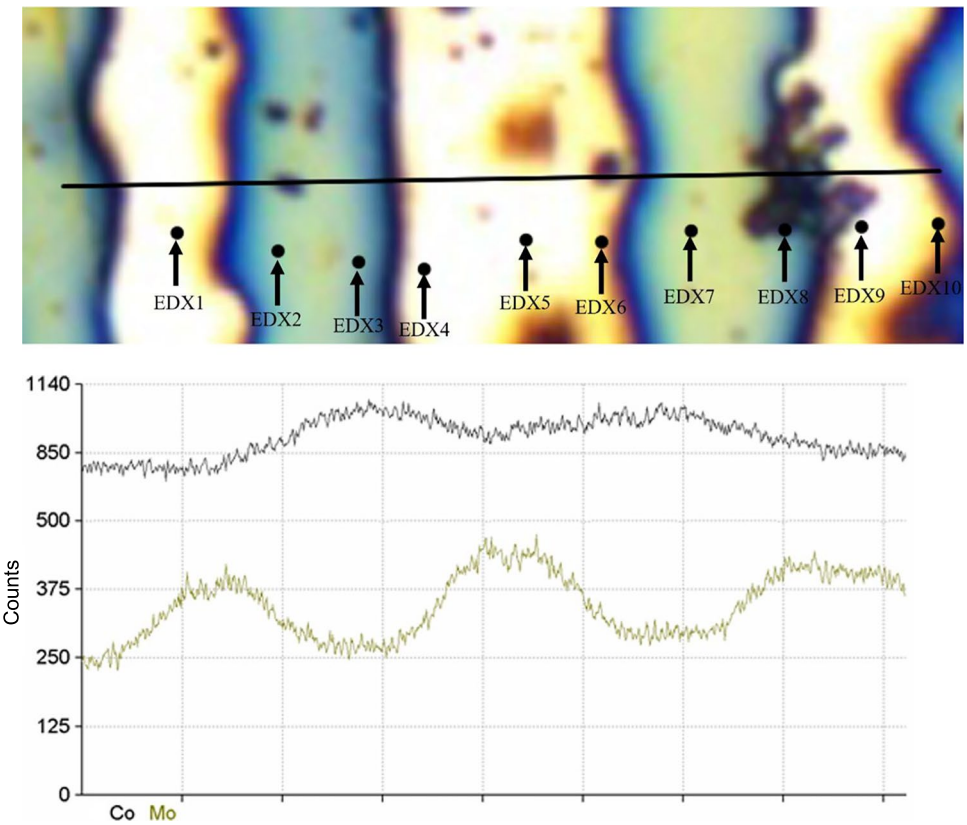

Fig. 5 EDX Line and point measurement of upper layer

Table 5 EDX point analysis of upper layers

Area	*Co*	*Cr*	*Ni*	*Mo*	*W*	*Fe*	*Mn*	*Si*
EDX 3	53.60	26.54	7.33	4.55	1.58	3.32	2.55	0.53
EDX 5	48.30	28.41	6.44	8.21	1.61	3.20	2.86	0.94
Avg. EDX(1–10)	51.26	27.62	7.11	5.71	1.46	3.39	2.73	0.66
Standard deviation	2.34	1.37	0.33	1.62	0.36	0.21	0.25	0.13

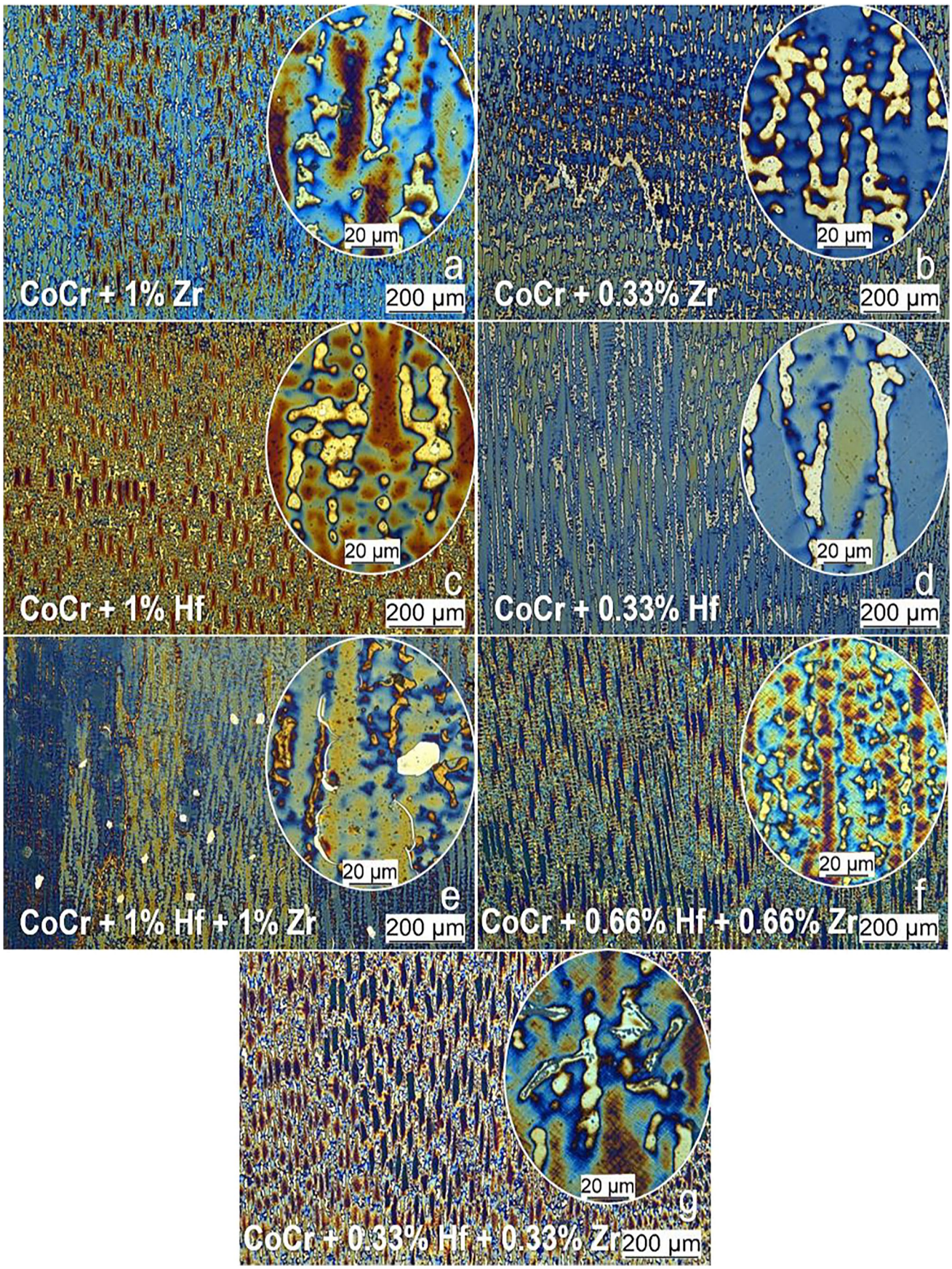
CoCr + 1% Zr
20 µm
a
200 µm
CoCr + 0.33% Zr
20 µm
b
200 µm
CoCr + 1% Hf
20 µm
c
200 µm
CoCr + 0.33% Hf
20 µm
d
200 µm
CoCr + 1% Hf + 1% Zr
20 µm
e
200 µm
CoCr + 0.66% Hf + 0.66% Zr
20 µm
f
200 µm
CoCr + 0.33% Hf + 0.33% Zr
20 µm
g
200 µm

◂**Fig. 6** Microstructure of **a** CoCr26Ni9Mo5W + 1% Zr, **b** CoCr26Ni9Mo5W + 0.33% Zr, **c** CoCr26Ni9Mo5W + 1% Hf, **d** CoCr26Ni9Mo5W + 0.33% Hf, **e** CoCr26Ni9Mo5W + 1% Zr + 1% Hf, **f** CoCr26Ni9Mo5 + 0.66% Zr + 0.66% Hf, **g** CoCr26Ni9Mo5 + 0.33% Zr + 0.33% Hf

3 Results and discussion

3.1 Microstructure and EDX analysis of CoCr26Ni9Mo5W

The Co–Cr initial alloy consists of a hypoeutectic dendritic structure typical for a Co–Cr alloy. Columnar primary dendrites have been formed with regularly distributed secondary dendrites, as well as a interdendritic region [25, 26], cf. Figure 4. On the contact zone between the layers, a fan-shaped morphology develops, whereby the individual layers can be easily distinguished from each other. According to the literature, the dendritic areas consist of eutectic Co–Cr solid solution, chromium-rich carbides ($M_{23}C_6$) and MC carbides. With elevated heat input, the size of the primary dendrites increases. At the boundary zones, this size decreases due to higher cooling rates compared to the centre of the weld.

For the deposition welding of CoCr26Ni9Mo5W, it can be seen that the averaged cobalt concentration over the individual EDX points is about 2.5% below nominal chemical composition. The EDX analysis shows that the concentration of cobalt has increased across the dendritic areas, Fig. 5 and Table 5. Thus, the cobalt content in point EDX3 (dendrite) is 53.6% and in point EDX 5 only 48.3%. The chromium content behaves in the opposite way and increases in the interdendritic areas. This is also in good agreement with the literature, in which chromium carbides are formed in the interdendritic region [27]. The EDX line analysis of molybdenum shows significant increases over the interdendritic area, cf. Figure 5.

3.2 Microstructure of modifications

This inhomogeneity over individual layers changes with all modified specimens. In the alloy modifications with 1% Zr (Fig. 6a) and 1% Hf (Fig. 6c), the quantity of secondary dendrites is reduced. In addition, significantly less interdendrites have formed, in which finely distributed precipitates can be found. These are cubic and rhombic carbides produced by zirconium and hafnium, respectively. Reducing zirconium to 0.33 wt.-% increases the homogeneity of the microstructure. A similar effect occurs with Co-Cr + 0.33% Hf, as the length of the primary dendrites grows, and their distribution becomes more uniform. Here, the size of the carbides is also slightly reduced. In the modification with 1% Hf + 1% Zr (Fig. 6e), the precipitates are larger and no longer limited to the residual solidification. They have a boulder and crescent shape. This is clearly different from the underlying layers, where the carbides are still enclosed by the dendrites. Consequently, the zirconium and hafnium carbides in the upper layers segregate due to repeated heating. In the modifications with 0.66% Hf + 0.66% Zr, as well as 0.33% Hf + 0.33% Zr, the precipitates are again surrounded by the interdendritic region. The number and width of the interdendritic region also increase with decreasing hafnium and zirconium content. At 0.66% Hf + 0.66% Zr, a columnar microstructure occurs, similar to 0.33% hafnium. In contrast, at 0.33% Hf + 0.33% Zr, a reticular structure similar to 0.33% Zr appears.

It is obvious that the chosen concentration ranges of the elements produce a distinct change in the structural morphology. In the case of the modifications with + 1 wt.-% Zr, a slightly increased porosity was detected by use of the IMS Client software, which is based on the fact that microcracks appear above the microstructure cross-section. No occurrence of these could be indicated at a lower content of 0.33 wt.-% Zr. Microcracks also occur in the combination 0.66% Hf + 0.66% Zr. However, these do not occur in the combinations with 1% and 0.33%. The assumption is that the contents of 0.33% the zirconium content is still too low and does not form microcracks, and at the high contents of 1%, the hafnium stabilizes this effect of zirconium.

3.3 Hardness measurements

The hardness measurements with HV 0.2 were performed for a more precise analysis of the microstructural constituents. It was measured over the cross-section of the sample and plotted with a mathematical smoothing filter for clarity of presentation, cf. Figure 7. The hardness measurements of the Co–Cr initial alloy and the modifications with 1% have a nearly steady curve at about the same level. The hardness is between 280 HV 0.2 and 320 HV 0.2. The hardness profile of CoCr26Ni9Mo5W + 1% Zr is below the level of the Co–Cr initial alloy. The reason is the microstructural constituents of the modification. The modification has significantly reduced the hard interdendritic regions, which decreases the hardness progression with HV 0.2. The hardness curve at a lower concentration of zirconium (CoCr26Ni9Mo5W + 0.33% Zr) increases again due to the higher amount of interdendritic areas compared to 1% Zr. For the combinations, 0.66% Hf + 0.66% Zr exhibits the highest hardness profile around the middle

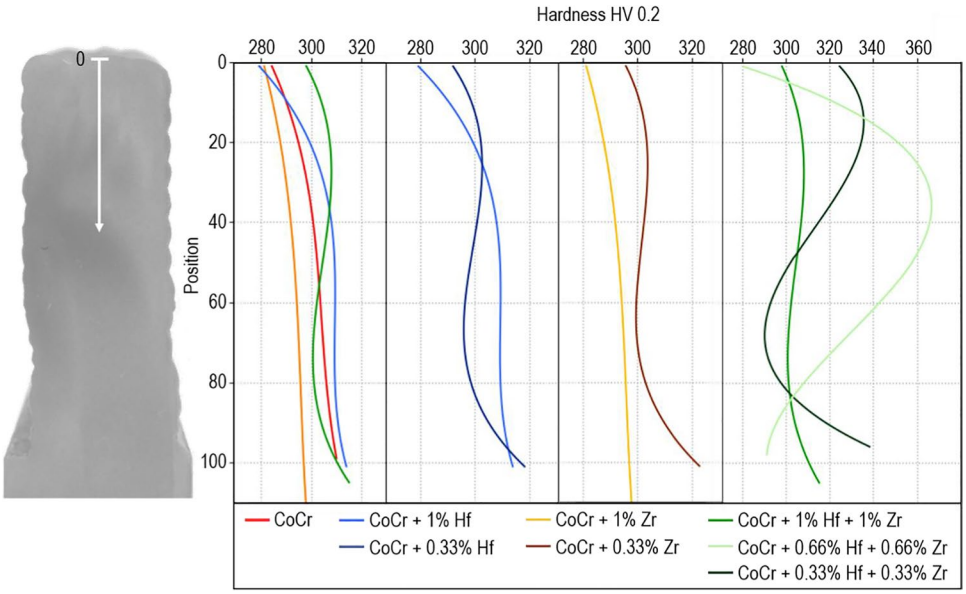

Fig. 7 Hardness measurement series HV 0.2 over the entire cross-section

layers. Numerous interdendritic regions are formed, which are tightly meshed, especially in the middle layers. In addition, hard carbides formed by zirconium and hafnium are enclosed in these. These two conditions cause the hardness progression to increase considerably compared to the other modifications.

The five individual hardness measurements with HV 10 are summarised in Fig. 8. These values show some differences to the small load hardness series measurements. With each modification, the hardness is enhanced compared to the Co–Cr initial alloy. The reason is that four of the individual measurements are located in the boundary areas of the sample cross-section and only one centrally point in the cross-section. In contrast, the boundary zones are almost not considered in the HV 0.2 hardness measurement series. Therefore, the arithmetic mean value of hardness of CoCr26Ni9Mo5W + 1% Zr is higher than of the Co–Cr initial alloy.

3.4 Machining analyses

The results of the finish-milling tests are shown exemplary in Fig. 9 for **a** one milling line and **b** one tool revolution. An extreme point represents one cutting engagement in each case.

The different heights of the force maxima or minima are due to the not exactly uniform geometry of the individual tool cutting edges due to slight deviations during the manufacturing process [28]. In each case, 5 milling lines were measured in the first and last third of a machined surface, and the mean value of the resulting cutting force was calculated. Consequently, the error bars represent the increase in cutting force during the process. The average height of the force maxima of the resulting cutting force F_r was evaluated, which refers to the theoretical number of cutting engagements for the sake of comparability. The results are shown in Fig. 10.

Both modifications of the Co–Cr initial alloy cause a significant reduction of the resulting cutting force for both machining processes, whereby the modification with 1% Zr induces the lowest resulting cutting force. The reduction in the resulting cutting force is due to the more homogeneous microstructure of both modifications compared with the Co–Cr initial alloy (cf. Figures 4 and 6). If conventional milling and USAM are compared, it exhibits that the resulting cutting force of the Co–Cr initial alloy and the modification of both process conditions are more or less equal. Slight deviations are found. However, the effect is smaller than scatter width and, therefore, not significant.

When considering the deviation of the resulting cutting force from the beginning to the end of one processed specimen surface, a very high increase of both milling conditions (USAM and conventional) is observed for the modification with 1% Zr. The modification with 1% Hf, on the other hand, causes a very low increase in the resulting cutting force during on processed area. Comparing both processes, USAM implies a significant lower increase of the resulting cutting force during the machining process compared to conventional milling for Co–Cr initial

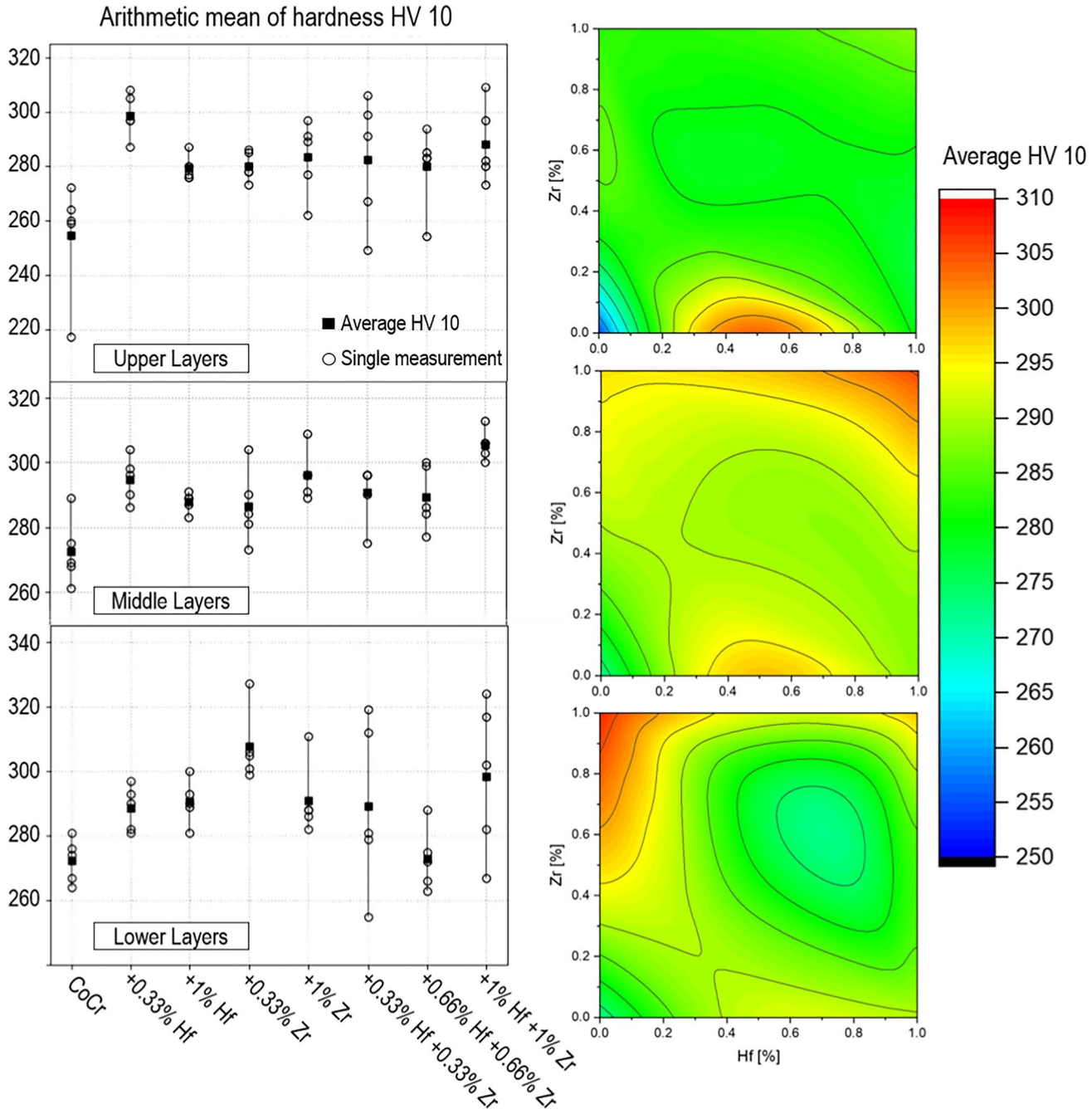

Fig. 8 Hardness measurement HV 10 of Co–Cr initial alloy and the modifications—presentation with scattering width (left) and via contour plots of avg. hardness vs. modification (right)

alloy and for the modification with 1% Hf. It is suggested that the stable machining process is responsible for these small variation of the forces during the process, which may ultimately lead to significant longer tool life. For the modification with 1% Zr, no difference for both process conditions is observable.

3.5 Surface integrity analyses

The results of the roughness measurement (normal to the feed direction) are shown in Fig. 11. The USAM causes a significantly lower arithmetic mean surface roughness *Ra* for all three materials compared to the conventional milling

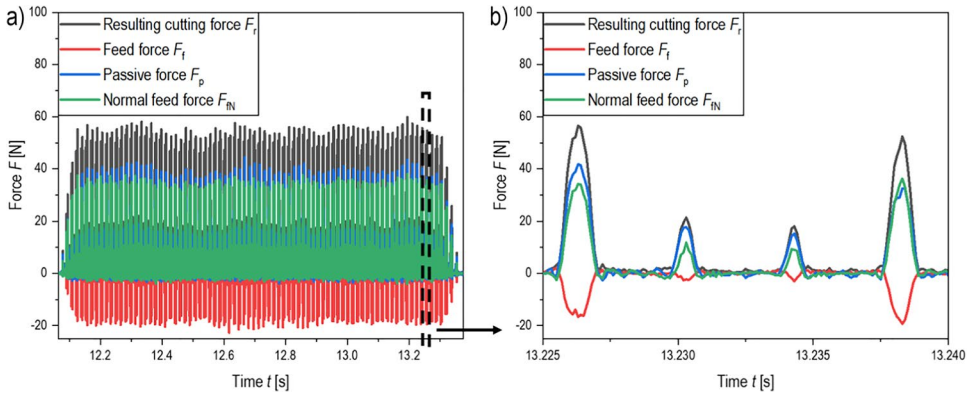

Fig. 9 Exemplary illustration of the resulting cutting force for **a** one milling line and **b** one tool revolution

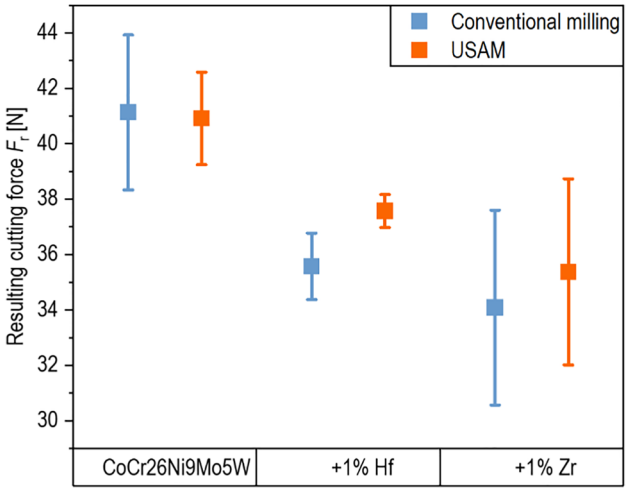

Fig. 10 Resulting cutting force F_r of the Co–Cr initial alloy, of the modification with + 1% Hf and of the modification with + 1% Zr

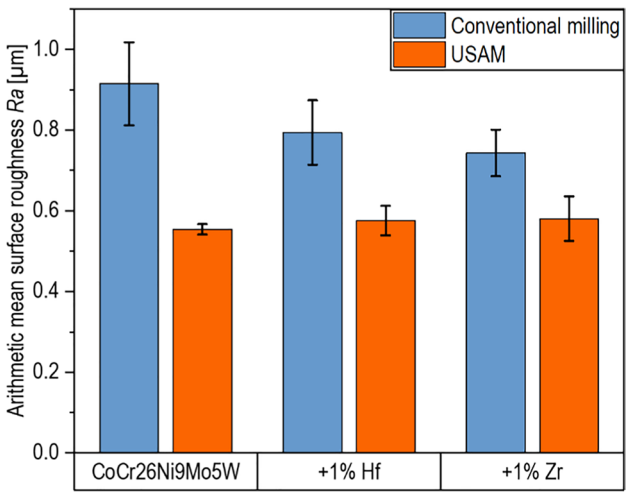

Fig. 11 Arithmetic mean surface roughness Ra of the Co–Cr initial alloy, the modification with + 1% Hf and the modification with + 1% Zr

process. The alloy modifications have no significant influence on the roughness regarding the USAM. If conventional milling is considered, a decreasing trend of the arithmetic mean surface roughness is observed for both modified alloys compared to the Co–Cr initial alloy.

In addition, the topography of the three materials was compared for USAM and conventional milling, cf. Figure 12. The surfaces of the conventional milling process (Fig. 12a, c, e) show a typical surface generated with a ball nose end mill, and the surfaces of the USAM (Fig. 12b, d, e) show the marks typical for ultrasonic assistance [29, 30]. The conventional milling process causes long grooves on the surface of the Co–Cr initial alloy, cf. Figure 12a. The long grooves are presumably due to carbide particles (chromium-rich carbides, $M_{23}C_6$ and MC carbides, cf. Section 3.1 detached from the workpiece, which are moved over the surface by the tool and consequently leave long grooves [31]. In contrast to the Co–Cr initial alloy, the surfaces of the two modifications with 1% Hf (Fig. 12c) and 1% Zr (Fig. 12e) of the conventional milling process exhibit a fractured surface. This could be the so-called tear defect, caused by the hafnium and zirconium carbides respectively, cf. Section 3.1. In this case, the carbide cracking phenomenon occurs during the machining process. The carbide particles are then pulled over the surface, leaving the tear defect [31, 32]. These defects are not visible on the surfaces of the specimens processed with USAM (Fig. 12b, d, f). One explanation could be the superimposed oscillation of the ultrasonic assistance. As Rinck et al. explain, the tool loses contact with the workpiece due to the superimposed oscillation. This consequently prevents the movement of the carbide particles over the surface [20], which results in a significant reduction of grooves and tear effects. The specimens processed with USAM show adhesion of chip particles for all alloy modifications, which could be due to a build-up edge (BUE) during milling. In this case,

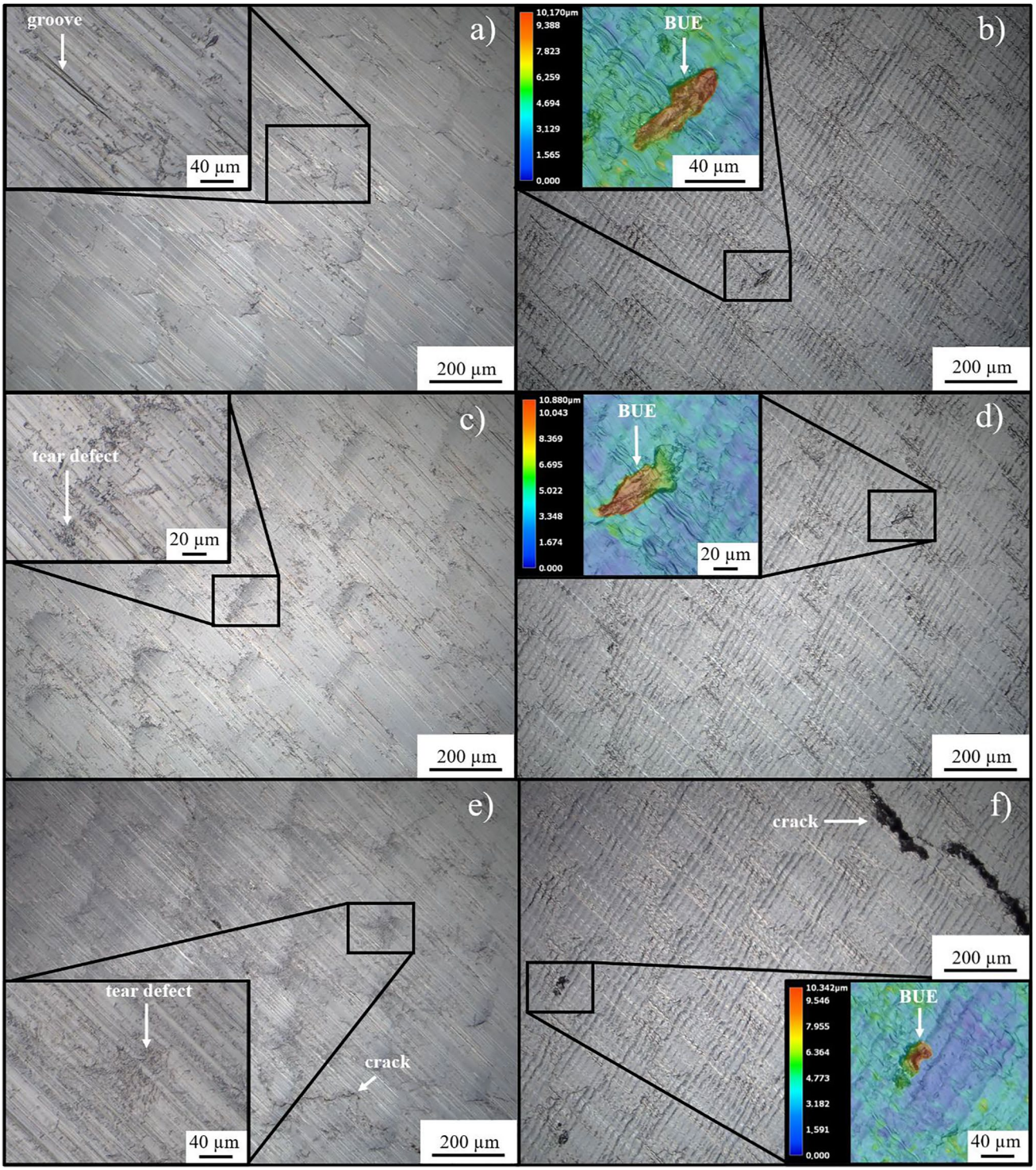

Fig. 12 Comparison of the topography of the Co–Cr initial alloy (**a**, **b**), the modification with 1% Hf (**c**, **d**) and the modification with 1% Zr (**e**, **f**) and of conventional milling (**a**, **c**, **e**) and USAM (**b**, **d**, **f**)

the BUE detaches from the tool cutting edge and adheres to the surface of the workpiece [31]. The microcracks (due to welding) of the modification with 1% Zr already explained in Section 3.2 are also observed on the finish milled surfaces of both machining processes, cf. Figure 12e and f. Overall, the surfaces of the USAM exhibit significant lower defect density compared to the conventional milling process.

4 Conclusion

The results show a clear influence of the alloying elements of hafnium and zirconium on the welded microstructure as well as on the machinability. The Co–Cr initial alloy was modified with different concentrations of the two elements.

1. At 1% concentration of the respective element, a homogeneous behaviour and ratio of dendritic and interdendritic area is shown.
2. Based on the changed microstructure morphology due to the microalloys, lower resulting cutting forces for subsequent machining are achieved for both modifications in comparison to the Co–Cr initial alloy.
3. In addition, the USAM results in machined surfaces with significant lower defect densities and roughness parameters compared to those processed with conventional milling.
4. 1% Zr leads to an increased number of microcracks across the microstructure cross-section. This is minimised with a lower mass-% of 0.33 still having a positive effect on the microstructure.
5. Adding + 1% Zr and + 1% Hf results in larger carbides floating in the upper layers. This composition should be investigated further.
6. The comparison of the hardness measurement of the Co–Cr initial alloy and all modifications shows that the high hardness of Co–Cr alloy is maintained or even slightly increased. It can be assumed that the excellent wear resistance properties of the Co–Cr alloy are maintained. This should be further investigated in future studies.

Acknowledgements The IGF project IGF No. 20.979 N (DVS 01.3211) of the Research Association of the DVS was supported by the Federal Ministry for Economic Affairs and Energy by the AiF as part of the program for support of the cooperative industrial research (IGF) on the basis of a decision by the German Bundestag.

Funding Open Access funding enabled and organized by Projekt DEAL. The companies involved in the project committee provided funding and support, in particular Deloro Wear Solutions GmbH, ECKART GmbH and S3 Handel und Dienstleistungen UG for providing the welding powder and WOLF Werkzeugtechnologie GmbH for providing the milling tools.

Declarations

Conflict of interest The authors declare no competing interests.

References

1. Sims C, Stoloff W, Hagel W (1987) Superalloys II – high-temperature materials for aerospace and industrial power. Wiley
2. Berns H, Fischer A (1993) Tribological stability of metallic materials at elevated temperatures. Wear 162–164:441–449. https://doi.org/10.1016/0043-1648(93)90528-t
3. Li Z (1989) Raabe D (2017) Strong and ductile non-equiatomic high-entropy alloys: design, processing, microstructure, and mechanical properties. JOM 69(11):2099–2106. https://doi.org/10.1007/s11837-017-2540-2
4. Kuzucu V, Ceylan M, Çelik H, Aksoy İ (1997) Microstructure and phase analyses of Stellite 6 plus 6 wt.% Mo alloy. J Mater Process Technol 69(1–3):257–263. https://doi.org/10.1016/s0924-0136(97)00027-7
5. Gupta KP (2005) The Co-Cr-Mo (cobalt-chromium-molybdenum) system. J Phase Equilib Diffus 26(1):87–92. https://doi.org/10.1361/15477030522608
6. Berns H (1998) Hartlegierungen und Hartverbundwerkstoffe – Gefüge, Eigenschaften, Bearbeitung. Springer, Anwendung
7. Zangeneh S, Farhangi H (2010) Influence of service-induced microstructural changes on the failure of a cobalt-based superalloy first stage nozzle. Mater Des 31(7):3504–3511. https://doi.org/10.1016/j.matdes.2010.02.021
8. Park JB, Jung K-H, Kim KM, Son Y, Lee J-I, Ryu JH (2018) Microstructure of As-cast Co-Cr-Mo alloy prepared by investment casting. J Korean Phys Soc 72(8):947–951. https://doi.org/10.3938/jkps.72.947
9. Bettini E, Eriksson T, Boström M, Leygraf C, Pan J (2011) Influence of metal carbides on dissolution behavior of biomedical CoCrMo alloy: SEM TEM and AFM studies. Electrochimica Acta 56(25):9413–9419. https://doi.org/10.1016/j.electacta.2011.08.028
10. Lin Z, Ya W, Subramanian VV, Goulas C, di Castri B, Hermans MJM, Pathiraj B (2020) Deposition of Stellite 6 alloy on steel substrates using wire and arc additive manufacturing. Int J Adv Manuf Technol 111(1–2):411–426. https://doi.org/10.1007/s00170-020-06116-w
11. Giacchi JV, Morando CN, Fornaro O, Palacio HA (2011) Microstructural characterization of as-cast biocompatible Co–Cr–Mo alloys. Mater Charact 62(1):53–61. https://doi.org/10.1016/j.matchar.2010.10.011
12. Frazier WE (2014) Metal additive manufacturing: a review. J Mater Eng Perform 23(6):1917–1928. https://doi.org/10.1007/s11665-014-0958-z
13. Schroepfer D, Treutler K, Boerner A, Gustus R, Kannengiesser T, Wesling V, Maus-Friedrichs W (2021) Surface finishing of hard-to-machine cladding alloys for highly stressed components. Int J Adv Manuf Technol 114(5–6):1427–1442. https://doi.org/10.1007/s00170-021-06815-y
14. Shokrani A, Dhokia V, Newman ST (2012) Environmentally conscious machining of difficult-to-machine materials with regard to cutting fluids. Int J Mach Tools Manuf 57:83–101. https://doi.org/10.1016/j.ijmachtools.2012.02.002
15. Alexander I, Vladimir G, Petr P, Mihail K, Yuriy I, Andrey V (2016) Machining of thin-walled parts produced by additive manufacturing technologies. Procedia CIRP 41:1023–1026. https://doi.org/10.1016/j.procir.2015.08.088

16. Abbasi SM, Morakabati M, Mahdavi R, Momeni A (2015) Effect of microalloying additions on the hot ductility of cast FeNi36. J Alloy Compd 639:602–610. https://doi.org/10.1016/j.jallcom.2015.03.167
17. Lizzul L, Sorgato M, Bertolini R, Ghiotti A, Bruschi S (2020) Influence of additive manufacturing-induced anisotropy on tool wear in end milling of Ti6Al4V. Tribology Int 146. https://doi.org/10.1016/j.triboint.2020.106200
18. Lizzul L, Bertolini R, Ghiotti A, Bruschi S (2020) Effect of AM-induced anisotropy on the surface integrity of laser powder fused Ti6Al4V machined parts. Procedia Manuf 47:505–510. https://doi.org/10.1016/j.promfg.2020.04.149
19. Ulutan D, Ozel T (2011) Machining induced surface integrity in titanium and nickel alloys: a review. Int J Mach Tools Manuf 51(3):250–280. https://doi.org/10.1016/j.ijmachtools.2010.11.003
20. Rinck PM, Gueray A, Kleinwort R, Zaeh MF (2020) Experimental investigations on longitudinal-torsional vibration-assisted milling of Ti-6Al-4V. Int J Adv Manuf Technol 108(11–12):3607–3618. https://doi.org/10.1007/s00170-020-05392-w
21. Ni C, Zhu L, Liu C, Yang Z (2018) Analytical modeling of tool-workpiece contact rate and experimental study in ultrasonic vibration-assisted milling of Ti–6Al–4V. Int J Mech Sci 142–143:97–111. https://doi.org/10.1016/j.ijmecsci.2018.04.037
22. Liu X-F, Wang W-H, Jiang R-S, Xiong Y-F, Lin K-Y (2020) Tool wear mechanisms in axial ultrasonic vibration assisted milling in-situ TiB2/7050Al metal matrix composites. Adv Manuf 8(2):252–264. https://doi.org/10.1007/s40436-020-00294-2
23. Leistner E, Weck E (1982) Metallographische Anleitung zum Farbätzen nach dem Tauchverfahren, Teil 2: Farbätzmittel nach Beraha uund ihre Abwandlungen, vol Fachbuchreihe. Deutscher Verlag für Schweißtechnik, Schweißtechnik
24. Geometrische Produktspezifikation (GPS) – Oberflächenbeschaffenheit: Tastschnittverfahren – Benennungen, Definitionen und Kenngrößen der Oberflächenbeschaffenheit (2010). DIN EN ISO 4287. https://doi.org/10.31030/1699310
25. Gholipour A, Shamanian M, Ashrafizadeh F (2011) Microstructure and wear behavior of stellite 6 cladding on 17–4 PH stainless steel. J Alloy Compd 509(14):4905–4909. https://doi.org/10.1016/j.jallcom.2010.09.216
26. Podrez-Radziszewska M, Haimann K, Dudziński W, Morawska-Sołtysik M (2010) Characteristic of intermetallic phases in cast dental CoCrMo alloy. Arch Foundry Eng 10(3/2010):51–56
27. Xue L (2018) Chapter 16 - Laser consolidation—a rapid manufacturing process for making net-shape functional components. In: Lawrence J (ed) Advances in Laser Materials Processing (Second Edition). Woodhead Publishing, pp 461–505. https://doi.org/10.1016/B978-0-08-101252-9.00016-9
28. Richter T, Schröpfer D, Rhode M, Börner A (2020) Influence of modern machining processes on the surface integrity of high-entropy alloys. IOP Conf Ser Mater Sci Eng 882:012016
29. Ahmed F, Ko TJ, Kurniawan R, Kwack Y (2021) Machinability analysis of difficult-to-cut material during ultrasonic vibration-assisted ball end milling. Mater Manuf Process 1–12. https://doi.org/10.1080/10426914.2021.1944194
30. Nespor D, Denkena B, Grove T, Pape O (2015) Surface topography after re-contouring of welded Ti-6Al-4V parts by means of 5-axis ball nose end milling. Int J Adv Manuf Technol 85(5–8):1585–1602. https://doi.org/10.1007/s00170-015-7885-5
31. Liu C, Ren C, Wang G, Yang Y, Zhang L (2015) Study on surface defects in milling Inconel 718 super alloy. J Mech Sci Technol 29(4):1723–1730. https://doi.org/10.1007/s12206-015-0345-1
32. Dosbaeva GK, Veldhuis SC, Elfizy A, Fox-Rabinovich G, Wagg T (2010) Microscopic observations on the origin of defects during machining of direct aged (DA) Inconel 718 superalloy. J Mater Eng Perform 19(8):1193–1198. https://doi.org/10.1007/s11665-009-9587-3